

# The influence of cooling rate and Fe/Cr content on the evolution of Fe-rich compounds in a secondary Al-Si-Cu diecasting alloy

**A Fabrizi<sup>a</sup> and G Timelli**

University of Padua, Department of Management and Engineering, Stradella S. Nicola, 3 - 36100 Vicenza, Italy

E-mail: <sup>a</sup>fabrizi@gest.unipd.it

**Abstract.** This study investigates the morphological evolution of primary  $\alpha$ -Al(Fe,Mn,Cr)Si phase in a secondary Al-Si-Cu alloy with respect to the initial Fe and Cr contents as well as to the cooling rate. The solidification experiments have been designed in order to cover a wide range of cooling rates, and the Fe and Cr contents have been varied over two levels. Metallographic and image analysis techniques have been used to quantitatively examine the microstructural changes occurring at different experimental conditions. The morphological evolution of the  $\alpha$ -Fe phase has been also analysed by observing deep etched samples. By changing the cooling rate,  $\alpha$ -Al<sub>15</sub>(Fe,Mn,Cr)<sub>3</sub>Si<sub>2</sub> dodecahedron crystals, as well as Chinese-script, branched structures and dendrites form, while primary coarse  $\beta$ -Al<sub>5</sub>(Fe,Mn)Si needles appear in the alloy with the highest Fe content at low cooling rates.

## 1. Introduction

From several decades, secondary Al-Si casting alloys have been widely used for the production of automotive components. A key-factor to be considered in the recycling of Al alloys consists in controlling the presence of impurities, such as the Fe level. The presence of Fe induces the precipitation of brittle Fe-rich compounds deleterious for the mechanical properties as well as the castability and the machinability of castings. In high-pressure diecast (HPDC) Al alloys, Fe-rich compounds crystallize with three distinct morphologies, such as needle-like, Chinese-script and star-like or polyhedral morphology [1]. According to the crystal structure and chemistry, the needle-like Fe-rich compounds are commonly referred as the monoclinic  $\beta$ -Al<sub>5</sub>FeSi phase, while Chinese-script and compact particles are generally indicated as  $\alpha$ -Al<sub>15</sub>(Fe,Mn)<sub>3</sub>Si<sub>2</sub>, or  $\alpha$ -Al<sub>12</sub>(Fe,Mn)<sub>3</sub>Si, phase with a body centred cubic (bcc) crystal structure [2]. However, morphology, size and volume fraction of each specific Fe-rich compound depend largely on the alloy composition and the solidification condition [3]. The Fe, Mn and Cr contents in the alloy, as well as their reciprocal ratio, significantly affect the morphology of the Fe-rich compounds [1,4]. It was found that a greater amount of needle-like particles is achieved for high Fe:(Mn+Cr) ratio, while more Chinese-script and/or polyhedral, star-like and blocky particles precipitate as the ratio decreases. As aforementioned, the morphology as well as the formation of Fe-rich compounds is also strongly affected by the cooling rate because of the diffusion and solubility variation of Fe, Mn and Cr during the solidification [5]. In the present work, the morphological evolution and the growth mechanism of primary  $\alpha$ -Fe phase in a secondary Al-Si-Cu alloy was studied as function of the cooling rate. 2D microstructural investigations coupled



to 3D characterizations were performed on HPDC specimens as well as on specimens solidified at lower cooling rates. Furthermore, the chemical composition of the base Al-Si-Cu alloy was varied by modifying the initial Cr and Fe contents.

## 2. Experimental procedure

Three secondary AlSi9Cu3 alloys with different Cr and Fe levels were used in this study. The melting procedure and the production of the HPDC specimens are described elsewhere [6]. The chemical compositions of the experimental alloys are given in table 1. About 80 g-piece was drawn from each HPDC alloy and remelted inside a cylindrical ceramic crucible with an inner diameter of 20 mm and a height of 80 mm by using an electric-resistance muffle furnace. The melting temperature was set at  $800 \pm 5^\circ\text{C}$  with 1 hour holding time in order to ensure homogeneity and, potentially, dissolution of the present intermetallics. After manually skimming, the molten metal was solidified according to two different cooling rates. For the first batch of specimens, the crucible was cooled in still air outside the furnace (hereafter called *medium cooling rate*); while the second batch was cooled more slowly to room temperature leaving the material inside the furnace at controlled cooling (hereafter called *low cooling rate*). The cylindrical as-cast samples were longitudinally sectioned and prepared for microstructural investigations by standard metallographic procedure. The microstructural characterization was performed by using optical microscope, scanning electron microscope (SEM), energy-dispersive spectroscopy (EDS) and electron back-scattered diffraction (EBSD). The microstructural scale was estimated by measuring the secondary dendrite arm spacing (SDAS) at equivalent positions in the as-cast specimens. The cooling rate,  $R$ , for each solidification condition was then determined from the SDAS values by using the equation:  $\text{SDAS} = 28.13 \cdot R^{-0.4}$  [7]. The 3D morphology of primary Fe-rich compounds was revealed by complete dissolution of Al matrix with a 20% NaOH water solution at  $65^\circ\text{C}$  for 15 minutes. Finally, the EDS analyses were carried out to study the chemical composition of the Fe-rich compounds with respect to the morphology and the cooling condition, while the combination of EDS and EBSD was performed to identify the phase and the crystallographic orientation of the compounds.

**Table 1.** Chemical compositions of the experimental alloys (wt.%);  $SF$  = Sludge Factor.

Alloy	Al	Si	Cu	Fe	Mn	Cr	Mg	Zn	Ni	Ti	Fe:Mn	$SF$
1	bal.	8.26	2.447	0.718	0.588	0.058	0.193	1.041	0.049	0.040	1.22	2.07
2	bal.	8.14	2.407	0.716	0.556	0.104	0.189	1.033	0.047	0.041	1.29	2.14
3	bal.	8.20	2.388	1.415	0.59	0.103	0.207	1.019	0.053	0.037	2.40	2.90

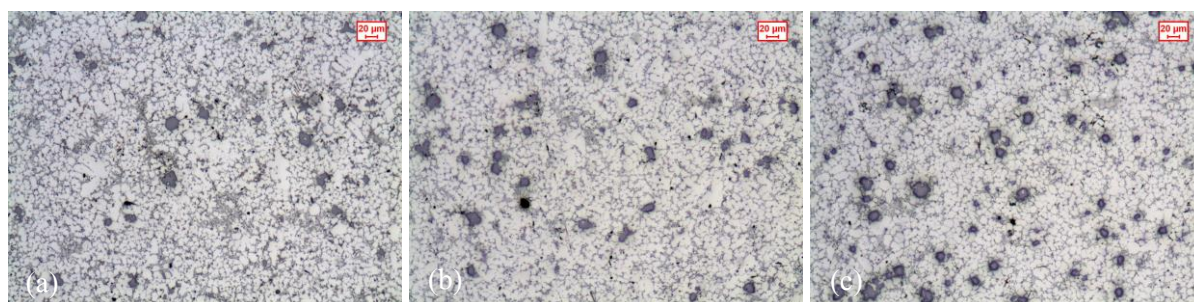
## 3. Results and discussion

The microstructures of the HPDC alloys are reported in figure 1. Primary polyhedral and star-like Fe-rich compounds with a mean diameter of  $\sim 20 \mu\text{m}$ , usually termed *sludge*, are uniformly distributed in all the alloys. The tendency of an Al alloy to form sludge particles strictly depends on the Fe, Mn and Cr contents according to the following empirical formula [8]:

$$\text{Sludge Factor (SF)} = (1 \times \text{wt.\%Fe}) + (2 \times \text{wt.\%Mn}) + (3 \times \text{wt.\%Cr}) \quad (1)$$

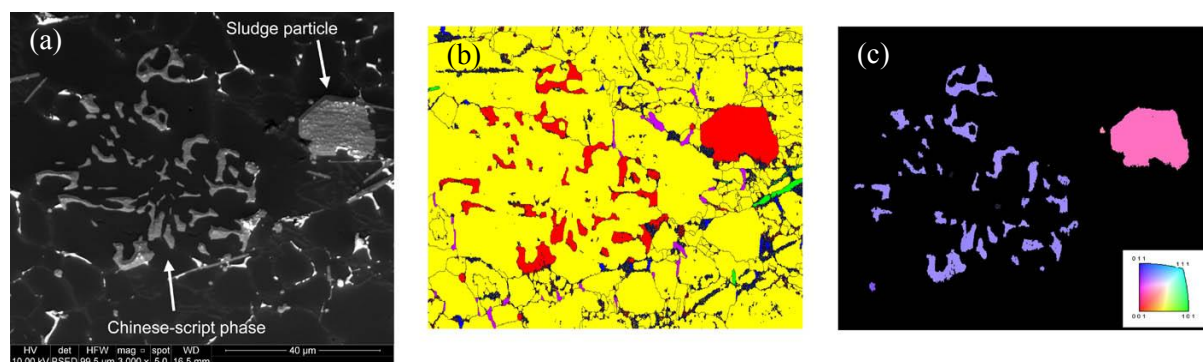
By comparing the different microstructures, the alloy 3 with the highest  $SF$  value shows a larger amount of primary Fe-rich compounds. Due to the high cooling rate in HPDC, all the alloys show a refined microstructure with very fine eutectic Si; the mean SDAS value results  $\sim 10 \mu\text{m}$  and no significant variation is noted among the alloys; moreover, the estimated cooling rate is about  $800^\circ\text{C/min}$ . Beside blocky particles, few primary Fe-rich compounds with a Chinese-script structure appear in all the experimental alloys (figure 2a). Generally, particles having a size comparable to the SDAS are considered primary (or pre-dendritic) phases. The EBSD investigations revealed that the

blocky particles and the Chinese-script structures well match a cubic structure (space group, *s.p.*, Pm-3) with the lattice parameter  $a \sim 1.26$  nm, associated to the  $\alpha$ -Fe phase (figure 2b). Further, from the orientation map of the  $\alpha$ -Fe phase in figure 2c, it results that all the distinct branched of the Chinese-script structure have identical crystallography orientation. The 3D characterization of deep-etched samples revealed the Chinese-script phase as a whole interconnected and branched structure [7,9].



**Figure 1.** Microstructures of the HPDC alloys: (a) alloy 1, (b) alloy 2 and (c) alloy 3.

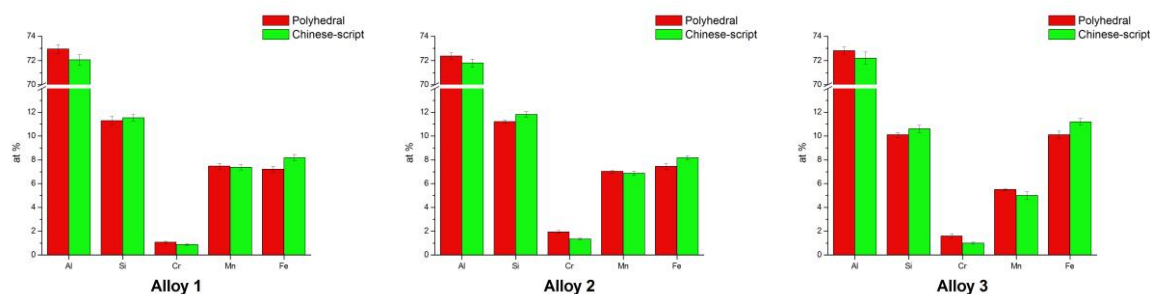
The chemical composition of the  $\alpha$ -Fe phase was studied as function of the morphology and the alloy composition through EDS, and the results are reported in figure 3. The stoichiometry of both Chinese-script and compact compounds can be considered consistent with both  $\alpha$ -Al<sub>12</sub>(Fe,Mn,Cr)<sub>3</sub>Si<sub>2</sub> and Al<sub>15</sub>(Fe,Mn)<sub>3</sub>Si<sub>2</sub> phases [10,11]. However, the Chinese-script morphology contains greater Si content and higher Fe:(Mn+Cr) ratio than the blocky particles. The EDS analyses also revealed that the chemical composition of  $\alpha$ -Fe phase depends on the alloy chemistry: higher the Cr and Fe levels in the alloys (alloys 2 and 3, respectively), higher the Cr and Fe contents in the Fe-rich compounds, regardless to their morphology.



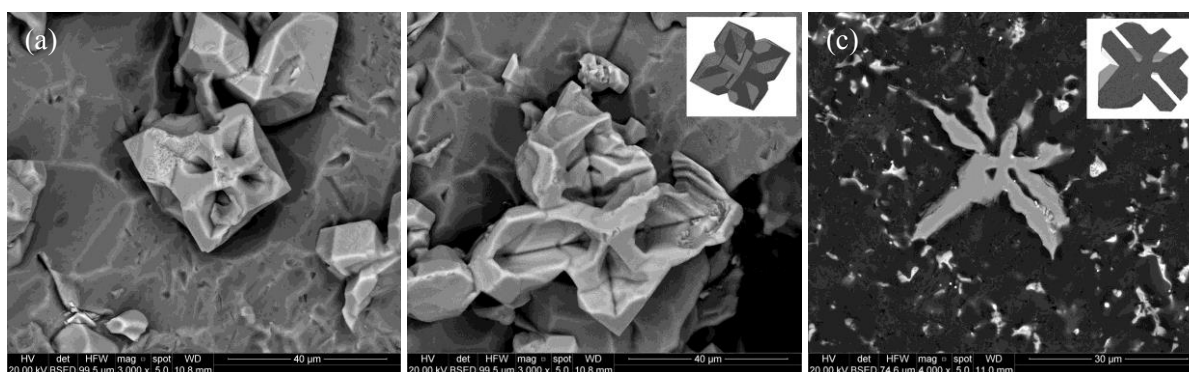
**Figure 2.** (a) SEM micrograph showing Fe-rich compounds with compact shape and Chinese-script morphology; corresponding (b) EBSD phase map (yellow =  $\alpha$ -Al (cubic, *s.p.* Fm-3m); red =  $\alpha$ -Fe (cubic, *s.p.* Pm-3); green =  $\beta$ -Fe (monoclinic, *s.p.* 2/m); blue = Al<sub>2</sub>Cu (tetragonal; *s.p.* I4/mcm); violet = Si) and (c) orientation map of  $\alpha$ -Fe phases.

Nevertheless, due to reciprocal substitution of Fe, Mn and Cr atoms in the cubic lattice of the  $\alpha$ -Fe phase, the total Fe+Mn+Cr content remains approximately constant for all the distinct morphologies. At high magnification, it is observed how many eutectic Si particles lie along the blocky Fe-rich compounds, suggesting blocky compounds constitute suitable site for nucleation of Si crystals. On the other hand, the Chinese-script compounds are separated from the eutectic Si through the  $\alpha$ -Al phase suggesting a peritectic reaction occurred. Concerning the blocky morphology of Fe-rich compounds, it has been recently found that most of the polyhedral and star-like 2D-morphologies derive from regular

or hollowed rhombic dodecahedron with a cavity on all the 12 rhombic facets, respectively [12]. The rhombic dodecahedron has totally 14 vertices, six of them are located on the three orthogonal axes and they correspond to the intersection common point of the four facets belonging to  $\{011\}$  crystal planes. After dissolution of  $\alpha$ -Al matrix by deep-etching, some hollowed dodecahedrons seem to exhibit an initial (figure 4a) or more advanced growth of the tips on the six different vertices, extending on the orthogonal, cube-edge  $\langle 100 \rangle$  directions (figure 4b). A 3D reconstruction of degenerated hollowed dodecahedron was carried out and insert in figure 4b. The relative cross-section of the 3D reconstruction seems to properly correspond to the observed 2D morphology (figure 4c).



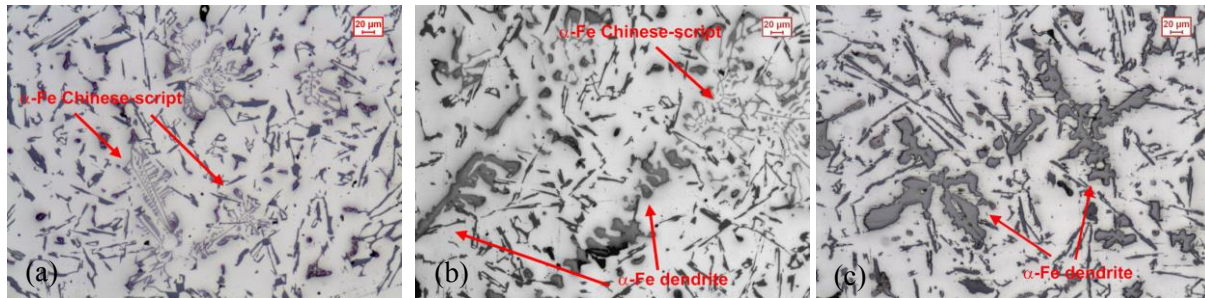
**Figure 3.** Chemical compositions (at.%) of  $\alpha$ -Fe phase as function of the different morphologies in the experimental alloys.



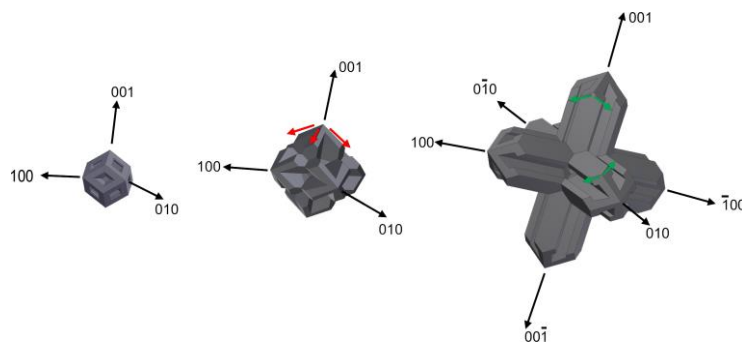
**Figure 4.** 3D microstructures of hollowed dodecahedron with (a) initial and (b) advanced growth of tips along orthogonal directions; (c) 2D morphology of a degenerated star-like structure. In the insets, the 3D CAD model and the associated cross-section are shown.

Figure 5 illustrates the typical microstructures of as-cast alloys solidified at *medium cooling rate*. In general, it can be clearly seen that the microstructural scale increased with respect to HPDC alloys; the mean SDAS value raises to  $\sim 40 \mu\text{m}$  for all the analysed alloys and the estimated cooling rate decreases to  $25^\circ\text{C/min}$ . The Fe-rich compounds show mainly Chinese-script morphology in alloys 1 and 2 but occasionally they assume a skeleton- or dendrite-like morphology. The fraction of coarse dendrites increases with the Cr content and even more with the Fe level. Considering the 3D morphology of the  $\alpha$ -Fe dendrites, a morphological evolution from the hollowed dodecahedron model to coarse dendrite is proposed (figure 6). By continuous growing of the tips on the six vertices during crystal growth, the primary dendrite arms can be formed along preferential  $\langle 100 \rangle$  direction and, further, secondary and ternary branches can be created from the primary arms growing along the orthogonal directions (figure 6c). The EDS results show that the chemical composition of the two types of  $\alpha$ -Fe compounds slightly differs. In general, the Chinese-script compounds show higher Fe content than the dendrites; further, the chemical composition of the  $\alpha$ -Fe phase is sensitive to the initial composition of the melt, as previously observed in the HPDC alloys. At the *low cooling rate*, the microstructural scale

of the alloys further increases (figure 7): in fact, the mean SDAS value is  $\sim 110 \mu\text{m}$  and the eutectic Si particles appear as coarse platelets while the cooling rate reaches  $\sim 2^\circ\text{C}/\text{min}$ . The previous coarse dendrites disappear and large blocky Fe-rich particles with an average size of  $\sim 350 \mu\text{m}$  are revealed at the bottom of the specimens. As reported by Shabestri et al. [11], primary  $\alpha$ -Fe crystals forming at temperatures above the liquidus cause gravity segregation due to their higher density. Furthermore, the Chinese-script structures become larger in the alloys 1 and 2. Comparing the microstructures in figure 5 with those resulting at low cooling rate (figure 7), it is evident that the secondary arm spacing of the Chinese-script phase increases as the cooling rate decreases.



**Figure 5.** Microstructures of as-cast (a) alloy 1, (b) alloy 2 and (c) alloy 3 solidified at medium cooling rate;  $\alpha$ -Fe Chinese-script compounds and coarse  $\alpha$ -Fe dendrites are indicated.



**Figure 6.** Schematic representation of the morphology evolution of primary  $\alpha$ -Fe compounds from hollowed dodecahedron to coarse dendrite. The growth direction of secondary and ternary arms are indicated by red and green arrows, respectively.

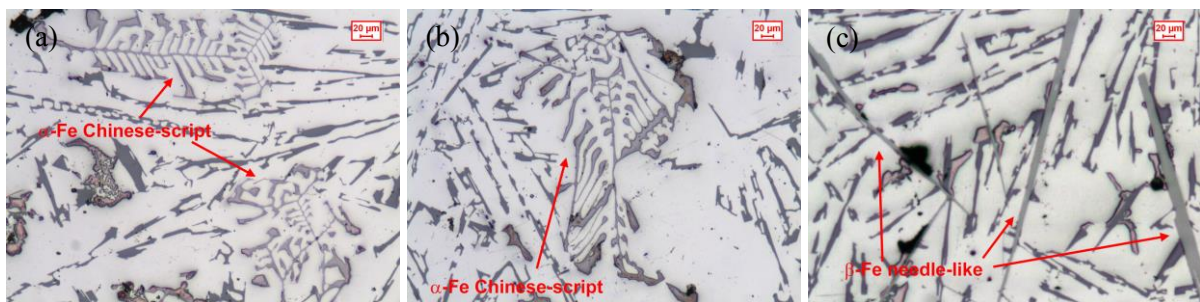


**Figure 7.** Microstructures of as-cast (a) alloy 1, (b) alloy 2 and (c) alloy 3 at low cooling rate:  $\alpha$ -Fe Chinese-script compounds and  $\beta$ -Fe needle-like particles precipitate.

As shown in figure 7c, coarse primary needle-like phases appear in the alloy 3 with the highest Fe:Mn ratio. According to the EDS analyses, the stoichiometry of the needle-like structures is  $\text{Al}_5(\text{Fe,Mn})\text{Si}_{1.4}$  and then identified as  $\beta$ -Fe phase. By considering the 2D and 3D microstructural

investigations, an explanation of the growth mechanism and morphology evolution of primary  $\alpha$ -Fe phase is proposed. Generally, at high cooling rates, the great undercooling promotes the formation of numerous and fine  $\alpha$ -Fe nuclei. The initial growth of these nuclei is diffusion controlled and, at this stage, the radial growth rate of such isolated seeds is fully isotropic. This leads to the formation of spherical primary  $\alpha$ -Fe phase. As the solidification proceeds, the nuclei grow and the cubic unit cells of  $\alpha$ -Fe phase can arrange spontaneously by growing in a faceted manner and by forming a rhombic dodecahedral structure. However, during the growth process, the  $\alpha$ -Fe crystal might exceed a critical size losing its stability. The growth velocity of the edges can prevail on the growth rate of the rhombic facets and, consequently, the formation of cavities at the facets' centres might occur (*skeletal growth* [13]), thus, hollowed rhombic dodecahedrons can form. Under such solidification conditions, the advancing growth of primary  $\alpha$ -Fe crystals is interrupted as the  $\alpha$ -Al dendrites rapidly begin to form. On the contrary, at slower cooling rates but still far away from a steady-state condition, the further growth of the primary  $\alpha$ -Fe crystals can continue before Al-dendrite formation and, at a more advanced stage, the six orthogonal vertices of the hollowed dodecahedron begin to rapidly protrude leading to the development of primary dendrite arms. Subsequently, secondary arms can be generated from the primary ones in the four orthogonal planes, forming branching facets. A similar growth process was also observed for Si and  $\text{Mg}_2\text{Si}$  crystals [14,15]. However, further investigations need to be performed in order to verify the growth mechanism of  $\alpha$ -Fe dendrites.

#### 4. Conclusions

The effects of cooling rate and Fe/Cr content on the formation and morphology evolution of primary Fe-bearing particles have been studied in a secondary Al-Si-Cu alloy. In the HPDC alloys, blocky compounds and small Chinese-script particles are detected. By reducing the cooling rate, large  $\alpha$ -Fe Chinese-script structures are identified to be the major intermetallic phase in the lower Fe content alloys, while coarse  $\alpha$ -Fe dendrites form by increasing the Cr and Fe level. At the slowest solidification regime,  $\alpha$ -Fe Chinese-script structures enlarge and coarse  $\alpha$ -Fe crystals grow and sediment at the bottom of the molten bath. Primary needle-like  $\beta$ -Fe particles result the dominant phase as the Fe:Mn ratio increases above 2. By studying the 3D morphologies of  $\alpha$ -Fe phase, a growth mechanism is presented to support the morphological transition of initial dodecahedral particles to coarse dendrites or to coarse crystals by varying the solidification conditions.

#### References

- [1] T Narayanan L A, Samuel F H and Gruzlesky J E 1994 *Metall. Mat. Trans. A* **25** 1761
- [2] Sweet L, Zhu S M, Gao S X, Taylor J A and Easton M A 2011 *Metall. Mater. Trans. A* **42** 1737
- [3] Makhlof M and Apelian D 2002, *Casting Characteristics of Aluminium Die Casting Alloys*, (Work Performed Under Contract No. DEFC07-99ID13716) pp 1-46
- [4] Gowri S and Samuel F H 1994 *Metall. Mater. Trans. A* **25** 437
- [5] Narayanan L A 1994, *Crystallization and dissolution studies of iron intermetallics in Al-Si alloys*, (McGill University, Montreal, Canada)
- [6] Timelli G, Ferraro S, Grosselle F, Bonollo F, Voltazza F and Capra L 2011 *Metall. Ital.* **103** 5
- [7] Sivarupan T, Caceres C H and Taylor J A 2013 *Metall. Mater. Trans. A* **44** 4071
- [8] Jorstad J L 1986 *Die Casting Engineer* **30** 30
- [9] Warmuzek M, Mrowka G and Sieniawski J 2004 *J. Mater. Process. Technol.* **157-158** 624
- [10] Shabestari S.G. 2004 *Mater. Sci. Eng. A* **383** 289
- [11] Shabestari S G and Gruzleski J E 1995 *Metall. Mater. Trans. A* **26** 995
- [12] Fabrizi A, Ferraro S and Timelli G 2014 *Shape Casting: 5th Int. Symp. 2014 - TMS 2014*, eds. M Tiryakioğlu, J Campbell, G Byczynski (Hoboken: John Wiley and Sons) pp 277-84
- [13] Li C, Wu Y Y, Li H and Liu X F 2011 *Acta Mater.* **59** 1058
- [14] Xu C L, Wang H Y, Liu C and Jiang Q C 2006 *J. Cryst. Growth* **291** 540
- [15] Qin Q D, Zhao Y G, Zhou W and Cong P J 2007 *Mater. Sci. Eng. A* **447** 186